Journal of Solid State Chemistry 292 (2020) 121723

Contents lists available at ScienceDirect

Journal of Solid State Chemistry

journal homepage: www.elsevier.com/locate/jssc

Investigation on structure, dielectric and magnetic properties of the four-layer Aurivillius phase $Pb_{1-x}Bi_{3.5+x}Nd_{0.5}Ti_{4-x}Mn_xO_{15}$ prepared via molten salt method

Zulhadjri *, Tio Putra Wendari, Upita Septiani, Syukri Arief

Department of Chemistry, Faculty of Mathematics and Natural Sciences, Universitas Andalas, Kampus Limau Manis, Padang, 25163, Indonesia

ARTICLE INFO

Keywords:
Aurivillius phase
Molten salt method
Dielectric properties
Magnetic properties
Double-exchange interaction

ABSTRACT

In this study, the four-layer Aurivillius phases, $Pb_{1-x}Bi_{3.5+x}Nd_{0.5}Ti_{4-x}Mn_xO_{15}$ (x = 0, 0.1, 0.3, and 0.5), were prepared by the molten salt method, in order to investigate the effects on crystal structure, morphology, dielectric and magnetic properties of varying x composition. XRD patterns revealed that of the all samples were single-phase products with an orthorhombic structure. The refinement result demonstrates a compressive unit cell volume with increasing x composition. Moreover, FTIR spectroscopy showed a single mode of BO_6 octahedra, and the shifting of this mode indicates that the Mn^{3+} ions occupy the perovskite B-site. The anisotropic plate-like grain was probed by SEM, the size of which showed an increase with a higher x composition, as the proportion of Bi^{3+} increases. The dielectric properties also increase with an increasing x composition, which results from the increasing structural distortion and grain size. The investigation of the magnetic properties indicates that the ferromagnetic behavior for the $x = 0.5$ sample, presumably originated from the double-exchange interactions between Mn^{3+} and Mn^{4+} and the spin canting of distorted $Mn(1)O_6$ octahedra via the Dzyaloshinskii–Moriya interaction. The formation of the mixed-valent Mn^{3+}/Mn^{4+} could likely be caused by the oxidizing environment, produced by the oxobasicity properties of the sulfate salt in this molten-salt method. Therefore, the multiferroic properties exhibited at room temperature were due to the optimum dielectric and magnetic properties that were obtained at $x = 0.5$.

1. Introduction

For many decades, ferroelectric materials have been proposed for potential applications such as data storage devices (RAM), energy storage capacitors, piezoelectric actuators, and ultrasonic transducers, primarily due to the combination of high dielectric properties, high Curie temperatures, large remnant polarization, and low dielectric loss [1,2]. Amongst them, the Aurivillius phase with these properties has gained much interest, as compared to other alternative perovskites compound. The rapid development of these industries requires rapid continuous enhancement of material properties such as multiferroic properties, which coexist with the ferroelectric and magnetic orders, are more superior to those of memory devices, in which the data is written by the electric field, and read out by magnetization [2,3].

The Aurivillius phases have emerged as promising candidates for this multiferroic compound because of their structural flexibility which can accommodate the various A- and B-site cation substitutions. The Aurivillius phase can be described structurally as the perovskite-like layers sandwiched between the bismuth oxides layers along the c-axis and can be represented by the general formula of $(Bi_2O_2)^{2+}(A_{m-1}B_mO_{3m+1})^{2-}$. Generally, the A is a mono-, di-, or trivalent cation with dodecahedral coordination, B is a transition metal cation (d^0) with octahedral coordination, and m is the number of octahedral layers [4].

In order to combine the ferroelectric and magnetic properties in Aurivillius phases, the introduction of magnetic transition metal with a partially filled d-shell (d^n) on the B-site is a subject of many ongoing studies [5–7]. It was reported that the well-known perovskite multiferroic $BiMnO_3$ exhibits coupling between ferroelectricity and ferromagnetism [3,8,9]. Therefore, the introduction of Mn^{3+} (d^4) into the B-site perovskite was expected to give rise to the multiferroic properties. However, the contradictory character between Mn^{3+} cations (d^4) and Ti^{4+} (d^0) possibly reduced the ferroelectricity, which was associated with the high leakage current [10]. It was widely reported that the substitution of Ln^{3+} for Bi^{3+} on the A-site perovskite layers suppresses the oxygen

* Corresponding author.
E-mail address: zulhadjri@sci.unand.ac.id (Zulhadjri).

https://doi.org/10.1016/j.jssc.2020.121723
Received 7 June 2020; Received in revised form 6 August 2020; Accepted 7 September 2020
Available online 10 September 2020

vacancy concentration, decreases the leakage current density and hence enhances the dielectric and ferroelectric properties [11,12]. Therefore, it was expected that the combination of both Nd^{3+} and Mn^{3+} substitution is to obtain the multiferroic Aurivillius compound.

Recently, we have reported on the synthesis of Ca-containing four-layer Aurivillius compound ($CaBi_4Ti_4O_{15}$) with the simultaneous substitution of both Ln^{3+} and Mn^{3+}, which were obtained the single-phase products. Both series of compounds exhibited the greater structural distortion and dielectric properties with increasing x (Mn^{3+}) composition [13,14]. In this work, we explore the Pb-containing four-layer Aurivillius ($PbBi_4Ti_4O_{15}$) since the Pb^{2+} ions with $6s^2$ lone pair electrons are expected to induce a higher structural distortion, which will likely favor the higher ferroelectricity. Lead bismuth titanate, $PbBi_4Ti_4O_{15}$ ($m = 4$), adopts a non-centrosymmetric orthorhombic structure with the $A2_1am$ space group as shown in Fig. 1a. This compound exhibits the ferroelectric properties with a high Curie temperature (T_c) of 801 K. The ferroelectricity is due to the $6s^2$ lone pair electrons associated with Pb^{2+} and Bi^{3+}, which induce highly distorted BO_6 octahedra as shown in Fig. 1b [9]. However, the magnetic behavior was reported as paramagnetic.

Most of the Aurivillius phase was synthesized using a conventional solid-state method. However, this method exhibited compositional inhomogeneity owing to the Bi^{3+} volatilization at high temperatures [6]. It is also difficult to control the morphology and grain size, which in turn affects the properties of Aurivillius [15]. Recently, we have reported on the multiferroic Aurivillius phase $Pb_{0.4}Bi_{2.1}La_{0.5}Nb_{1.7}Mn_{0.3}O_9$ synthesized by the molten salt method using K_2SO_4/Na_2SO_4 salt with the varying ratios of oxide to salt [16]. The single-phase product with the best ferroelectric and ferromagnetic properties was obtained for the molar ratio of 1:7. The salt fluxes as the reaction medium provide advantages such as lower-temperature synthesis, fast ionic diffusion, and high reaction rates.

Herein, we have synthesized the compounds of composition $Pb_{1-x}Bi_{3.5+x}Nd_{0.5}Ti_{4-x}Mn_xO_{15}$ ($x = 0$, 0.1, 0.3, and 0.5) using a molten salt method using K_2SO_4/Na_2SO_4 salt, which has not previously been reported. The crystal structure, morphology, dielectric and magnetic properties were also discussed in this work.

2. Experimental procedures

The four-layer Aurivillius phases $Pb_{1-x}Bi_{3.5+x}Nd_{0.5}Ti_{4-x}Mn_xO_{15}$ ($x = 0$, 0.1, 0.3, and 0.5) were synthesized by a molten salt method using a mixture of K_2SO_4/Na_2SO_4. The starting materials used were the high purity oxides of PbO, Bi_2O_3, Nd_2O_3, TiO_2, and Mn_2O_3 (Aldrich, $\geq$ 99.9%). The molar ratios of oxide to salt were 1:7 and the synthesis temperature method were as reported in Ref. [16]. The phase formation was determined using X-ray diffraction (XRD; Shimadzu XRD 7000) with Cu Kα

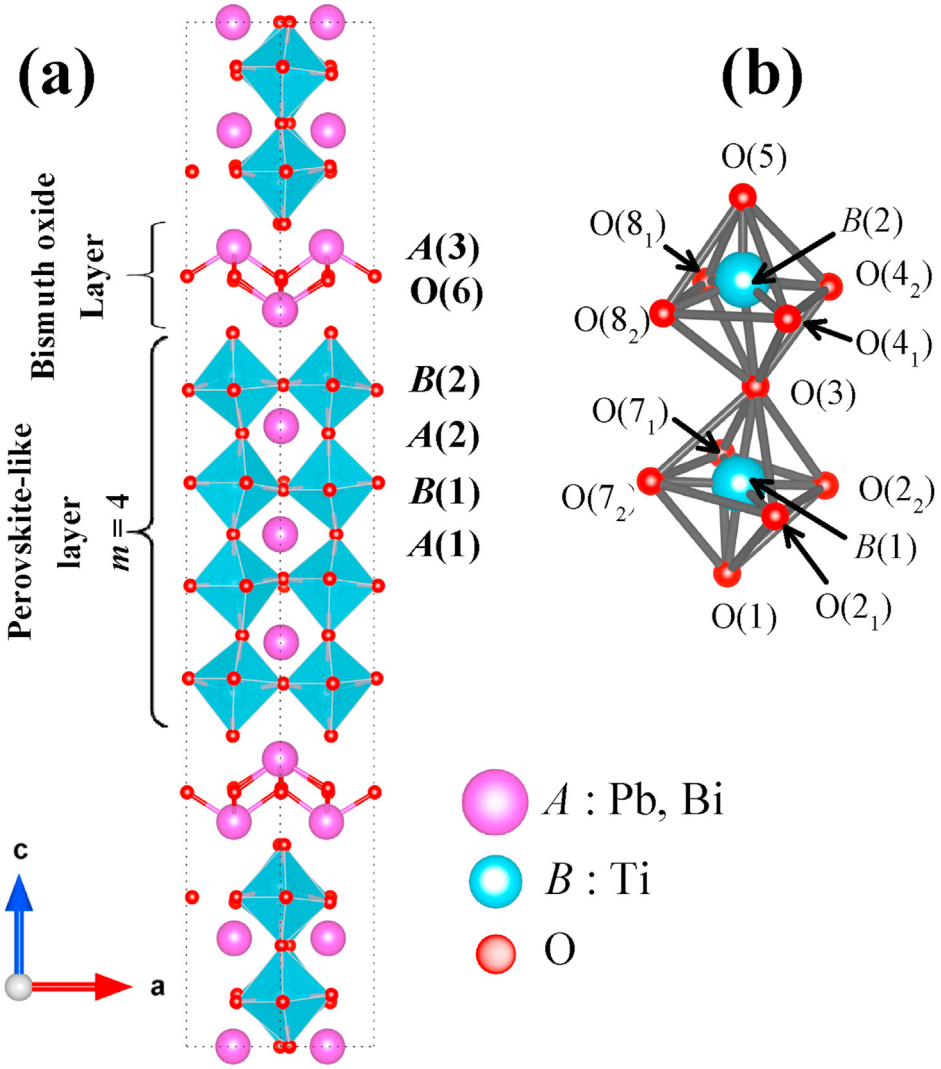

Fig. 1. (a) Crystal structure models of four-layer Aurivillius $PbBi_4Ti_4O_{15}$ phase viewed along the *ac*-plane. (b) View of distorted $B(1)O_6$ and $B(2)O_6$ octahedra projected along the c-axis. Structural parameters were taken from Ref. 9.

radiation (λ = 1.5418 Å). The Le Bail refinement method using the RIETICA program was performed to identify the crystal structure. FTIR spectroscopy was performed using a PerkinElmer 1600 FTIR spectrophotometer at room temperature. The grain morphology was observed using a scanning electron microscope (SEM; FEI INSPECT S50). The density was measured using the Archimedes method and the theoretical density was calculated from the refinement result. For the dielectric measurement, the final products were pressed into pellets with a diameter of 1 cm in and thickness 0.1 cm. The pellet sintered continuously at 500 °C and 900 °C for 3 h each. Both surfaces of sintered pellets were polished with silver conductive paste (Aldrich, 99%) to form the electrodes and dried at 423 K for 2 h. Capacitance and loss were measured as a function of frequency using a precision LCR-meter (Agilent 4980 A) with an amplitude of 1 V at 300 K. Magnetization as a function of the applied field were measured using a vibrating samples magnetometer (VSM; OXFORD 1.2H) at a temperature of 300 K.

3. Results and discussion

Fig. 2a shows the XRD patterns of $Pb_{1-x}Bi_{3.5+x}Nd_{0.5}Ti_{4-x}Mn_xO_{15}$ (x = 0, 0.1, 0.3, and 0.5) at room temperature. All XRD patterns can be well-matched with the standard XRD pattern of four-layer Aurivillius $PbBi_4Ti_4O_{15}$ (ICSD-96609). No additional peak was observed in all samples, confirming the formation of the single-phase products. This result shows that the substitution of 12.5% molar ratio La^{3+} for Bi^{3+} and 12.5% molar ratio Mn^{3+} for Ti^{4+} can be simultaneously substituted in $PbBi_4Ti_4O_{15}$ structure when the Pb:Bi ratio is adjusted accordingly. It was previously reported that the single-phase products of the four-layer Aurivillius compounds were obtained for the Mn substitution up to 15% using the molten salt method [9,13,14]. It was inferred that the substitution of Mn^{3+} for 15% could be possible.

Furthermore, the most intense diffraction peak of all samples corresponded to the (1 1 9) plane, coinciding with the (1 1 2m + 1) peak in the Aurivillius phase, whereas m = 4 refers to the number of layers. This peak gradually shifted towards the higher 2θ with an increasing x composition, as shown in the enlarged view of Fig. 2b, implying a decreased cell volume. The average crystallite size was calculated using the Scherrer equation [16]. The average crystallite size was found to decrease with an increase in x composition, which is approximately 54 nm, 52 nm, 50 nm, and 47 nm for x = 0, 0.1, 0.3, and 0.5, respectively. This result can be revealed with the increase in the full width at half maximum (FWHM) values as shown in Fig. 2c. The decreased crystallite size is correlated to the contraction of cell volume of crystal structure, as shown by the shift of the XRD peak [17].

The changes in cell parameters and cell volume were investigated by the Le Bail refinement method using the structural parameter of $PbBi_4Ti_4O_{15}$ with a space group $A2_1am$ as an initial model [9]. Le Bail fits to the XRD patterns of $Pb_{1-x}Bi_{3.5+x}Nd_{0.5}Ti_{4-x}Mn_xO_{15}$ are shown in Fig. 3. The good fit between the experimental and calculated patterns with a small difference between these two intensities demonstrates that all samples adopt the orthorhombic $A2_1am$ space group and this structure does not change with the varying x composition.

The refined lattice parameters and cell volume is shown in Fig. 4. The a lattice parameter slightly increase, whereas the b and c lattice parameters decrease as x composition increases, leading to the decrease in cell volume. Referring to the ionic radius of Pb^{2+} (1.49 Å) and Bi^{3+} (1.31 Å) for 12-fold coordination and the ionic radii of Mn^{3+} (0.645 Å) and Ti^{4+} (0.605 Å) for 6-fold coordination [18,19], the decreased cell volume is strongly affected by the increasing proportion of smaller Bi^{3+} and the decreasing proportion of larger Pb^{2+}, according to the nominal formula of $Pb_{1-x}Bi_{3.5+x}Nd_{0.5}Ti_{4-x}Mn_xO_{15}$. These compositional changes resulted in the higher distortion of the BO_6 octahedra, by which the structure becomes more orthorhombic [20,21]. This distortion led to the tilting of BO_6 octahedra along the a-axis, confirmed by the increased difference between the a and b lattice parameter [22]. The degree of distortion could be evaluated from the orthorhombicity ratio $(a-b)/(a+b)$. The orthorhombicity gradually increased with increasing x composition as shown in Fig. 4b, which revealed the increase in structural distortion. This is also consistent with the decrease in the tolerance factor (t) calculated for the perovskite-part structure [23]. The increase in distortion was driven both by the increase of $6s^2$ lone pair electrons of Bi^{3+} and the size mismatch between the A- and B-site cations [24,25]. The increase in distortion contributes to the increased ferroelectricity.

Furthermore, it is clearly observed in Fig. 4a that the c parameter decreased abruptly with the cell volume for x = 0.5. A decreased c parameter is generally associated with a shortening of the B–O bond distance as well as the BO_6 octahedra size. The significant decrease of c parameter in x = 0.5 might be further raised by the formation of smaller Mn^{4+} ions (0.54 Å) compared to Mn^{3+} (0.645 Å). A similar trend was also observed in $Ca_{1-x}Bi_{3+x}LaTi_{4-x}Mn_xO_{15}$, whereas the formation of Mn^{4+} caused a decrease in c lattice parameters and volume cell [14]. The existence of Mn^{4+} ions could also be expected to give rise to the magnetic ordering, as discussed further below.

Fig. 5a shows the IR spectra of $Pb_{1-x}Bi_{3.5+x}Nd_{0.5}Ti_{4-x}Mn_xO_{15}$ in the spectral range 600–1400 cm^{-1}, corresponding to the vibration modes of BO_6 octahedra (>200 cm^{-1}). A vibration mode at ~830 cm^{-1} was

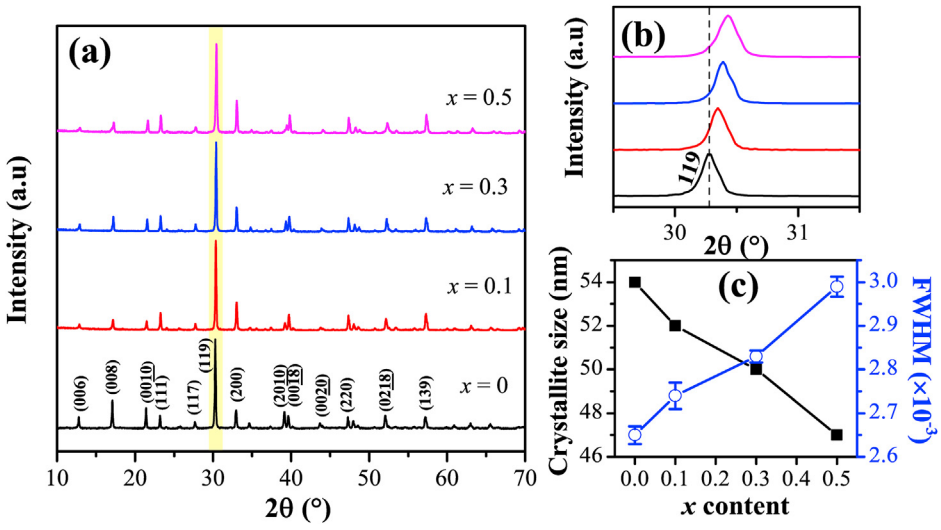

Fig. 2. (a) XRD patterns of $Pb_{1-x}Bi_{3.5+x}Nd_{0.5}Ti_{4-x}Mn_xO_{15}$ powders (x = 0, 0.1, 0.3, and 0.5). (b) The enlarged view of (1 1 9) XRD peak. (c) Comparison of crystallite size and FWHM peak.

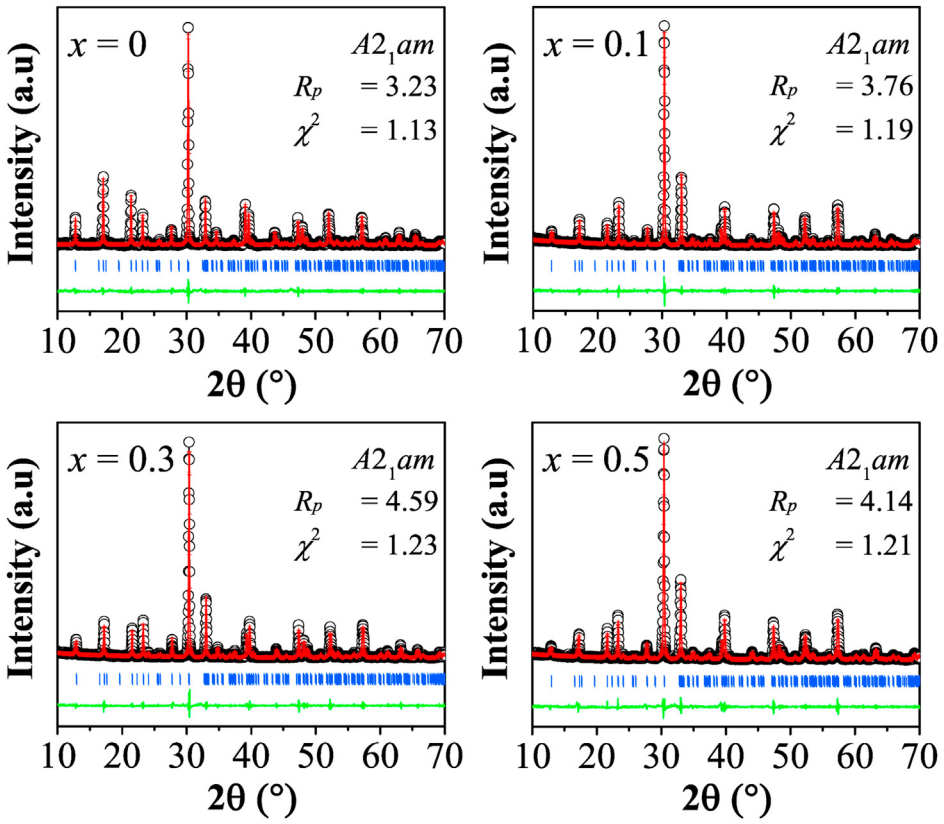

Fig. 3. Le Bail fits to XRD data for single-phase $Pb_{1-x}Bi_{3.5+x}Nd_{0.5}Ti_{4-x}Mn_xO_{15}$ and the reliability factor of refinement result. Observed XRD data (open circles), calculated data (red line), difference data (green line), and Bragg reflections of space group $A2_1am$ (blue tick). (For interpretation of the references to colour in this figure legend, the reader is referred to the Web version of this article.)

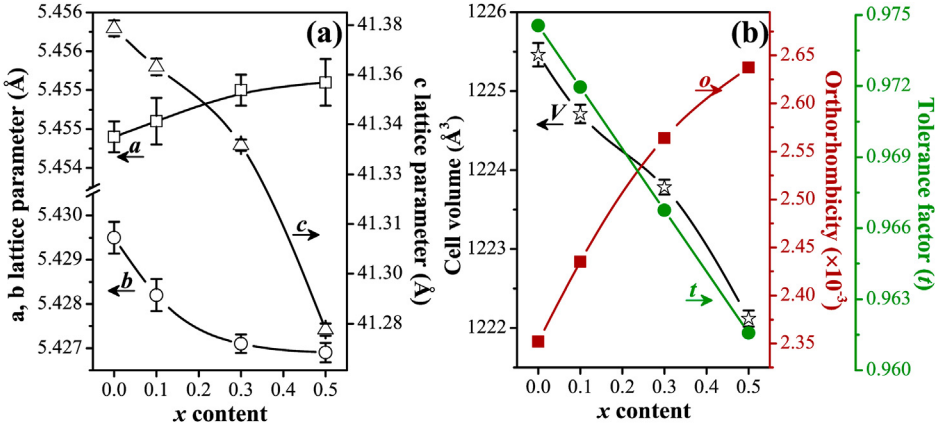

Fig. 4. (a) Refined lattice parameters of $Pb_{1-x}Bi_{3.5+x}Nd_{0.5}Ti_{4-x}Mn_xO_{15}$ (x = 0, 0.1, 0.3, 0.5). (b) Composition dependence of cell volume, orthorhombicity ratio and tolerance factor.

observed in the spectra of all samples, assigned to the symmetric *B*–O stretching mode of BO_6 octahedra in the perovskite layers [11]. The peak position and the full widths at half maximum (FWHM) of the IR spectra fitted using a Lorentzian model are shown in Fig. 5b. It was found that the peak shifted towards the lower wavenumber and became broader with the increase in x composition. The obvious shift of *B*–O mode was induced by the substitution of Mn^{3+} for Ti^{4+} since the chemical bond strength of the Mn–O bond (362 kJ/mol) is smaller than that of Ti–O (666.5 kJ/mol) [20,26]. The increase in FWHM value correlated to the increased compositional disorder of the *B*-site cations as the proportion of Mn^{3+} increased. Moreover, no traces of sulfate vibration mode around 970–995 cm^{-1} reveals that the salt does not chemically react with the product of this method.

SEM micrographs of $Pb_{1-x}Bi_{3.5+x}Nd_{0.5}Ti_{4-x}Mn_xO_{15}$ powder sample were shown in Fig. 6a-d. The typical plate-like grains of the Aurivillius phase were observed. The plate-like morphology was formed due to the lower surface energy along the (00*l*) planes, which lead to the preferential grain growth along the *a*–*b* plane [11]. The grain size was observed to increase with increasing x composition. The increase in grain size was associated with an increase in the proportion of Bi^{3+} since it has high ionic mobility and stimulates grain growth [20]. Fig. 6e shows that the density increased as x composition increased. The relative density of all samples were found to be greater than ~94% of the theoretical density, indicating the well-dense grains under this molten salt method.

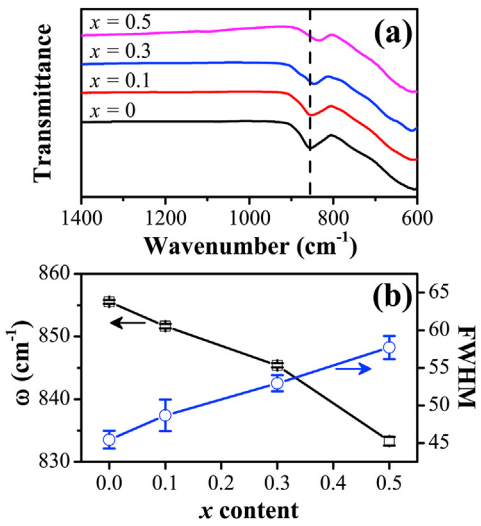

Fig. 5. (a) FTIR spectra of $Pb_{1-x}Bi_{3.5+x}Nd_{0.5}Ti_{4-x}Mn_xO_{15}$ ($x = 0$, 0.1, 0.3, 0.5) at room temperature. (b) Composition dependence of wavenumber and FWHM of *B*–O vibration mode.

Fig. 7 shows the dielectric constant (ε) and dielectric loss (tan δ) measured over various frequency ranges at room temperature (300 K). It was observed that the dielectric constant decreased as the frequency increased and became constant at high frequencies, which is typical behavior of ferroelectric materials [27]. At low frequencies, the contribution of different polarizations (*i.e.* dipolar, ionic, electronic, and space-charge) led to the higher dielectric constant. This was also caused by the accumulation of charge carriers at both surface and grain boundaries since it could not respond well to the applied field, also known as the Maxwell-Wagner effect [9]. Therefore, the stronger dispersion of dielectric constant with increasing *x* composition is likely due to the domination of the space-charge polarizations, arising from the increase in electron concentration of Mn ions [10,11]. Thus, the high dielectric constant at low frequencies arises from the combination of both intrinsic and extrinsic factors.

The decrease in dielectric constant at higher frequencies was due to the absence of different types of polarization and the conducting behavior. Thus, the magnitude of the dielectric constant at high frequencies is more reliable to reflect the intrinsic polarizability. The dielectric constant at 1 MHz was found to increase from 105.5 for $x = 0$ to 174.6, 200.8, and 245.1, respectively for the increase in *x* composition. The high dielectric constant at room temperature was associated with the ferroelectric behavior in all samples, which correlated to the $A2_1am$ orthorhombic symmetry. The increased ferroelectricity was attributed to the increased structural distortion, as revealed by the increasing orthorhombicity ratio and the decreasing tolerance factor (*t*). Besides, the increase in grain size allowed the domain to be polarized more easily, which also contributed to this magnitude [7,16].

The dielectric loss (tan δ) also exhibited a strong dispersive value at low frequencies as seen in Fig. 7b, which is due to the domination of space charge polarization effects. The dielectric loss at 1 MHZ was found to increase for $x = 0$, 0.1, 0.3, and 0.5 with value of 0.017, 0.057, 0.111, and 0.291, respectively, indicating the sample became more conductive. This was strongly affected by the increase in the electron concentration as the charged carriers by the substitution of Mn^{3+} for Ti^{4+}. Furthermore, the reduction in the number of grain boundaries subsequently contributed to the higher dielectric loss since it allowed easier electron migration [20].

To investigate the magnetic behavior, the magnetic field dependence of the magnetization (*M-H*) was performed at room temperature as shown in Fig. 8. The magnetic behavior was compared only for sample $x = 0$ and $x = 0.5$ since the sample of $x = 0.5$ exhibited the highest dielectric properties of these series and the maximum Mn composition was expected to provide the highest magnetic properties. The *M-H* curve of $x = 0$ exhibited a negative magnetization with no loop opening, demonstrating a typical diamagnetic behavior [7]. The $x = 0.5$ sample exhibited a non-linear fashion, and a narrow hysteresis loop can be observed in the inset of Fig. 8, indicating the existence of ferromagnetic behavior. The unpaired electrons of Mn cations were mainly responsible for the magnetic properties of $x = 0.5$. The unsaturated hysteresis loop indicated that the maximum applied magnetic field of 1 T was insufficient to completely arrange the spin orders. The saturated magnetization (M_s) and the remnant saturation (M_r) were 0.058 emu/g and 0.005 emu/g, respectively.

The ferromagnetism of $x = 0.5$ possibly originated from the existence of the double-exchange interactions in BO_6 octahedra. As shown in Fig. 1a, the four-layer Aurivillius phases contain two types of octahedral structures as the inner $B(1)O_6$ and the outer $B(2)O_6$, where the Mn^{3+} cations possibly occupy in both sites. It was previously reported that the magnetic transition cations preferentially occupy the inner site of $B(1)O_6$ octahedra with a lower distortion due to the high symmetry of the *d*-orbitals [5,9]. This preference for local ordering of magnetic ions was also observed previously by Raman spectroscopy [6,20]. Therefore, it can be inferred that Mn ions preferred to occupy the adjacent inner $B(1)O_6$ octahedra in this sample. Moreover, it has commonly been observed that

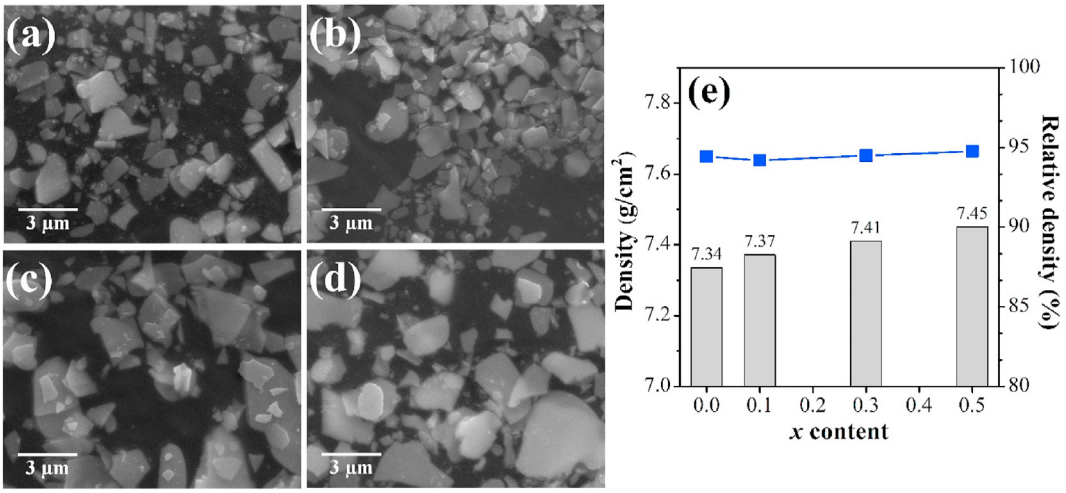

Fig. 6. SEM micrograph of $Pb_{1-x}Bi_{3.5+x}Nd_{0.5}Ti_{4-x}Mn_xO_{15}$ powders samples (a) $x = 0$ (b) $x = 0.1$ (c) $x = 0.3$ (d) $x = 0.5$ and (e) the density and relative density as a function of *x* composition.

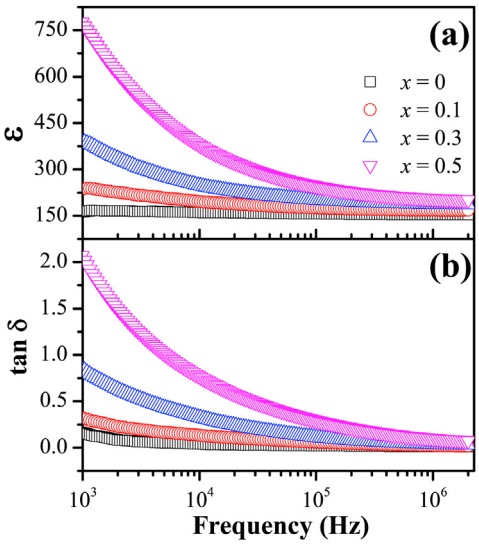

Fig. 7. (a) Dielectric constant (ϵ) and (b) dielectric loss (tan δ) of $Pb_{1-x}Bi_{3.5+x}Nd_{0.5}Ti_{4-x}Mn_xO_{15}$ ($x = 0$, 0.1, 0.3, and 0.5) as a function of frequency at room temperature.

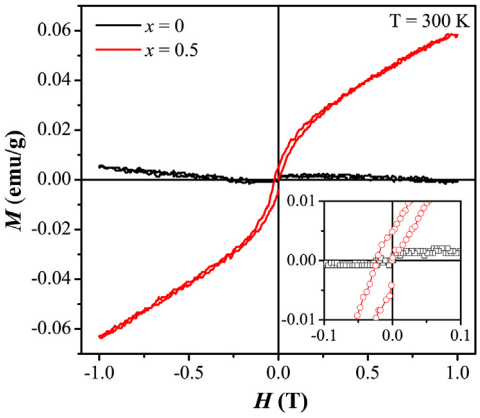

Fig. 8. *M–H* loops of $Pb_{1-x}Bi_{3.5+x}Nd_{0.5}Ti_{4-x}Mn_xO_{15}$ ($x = 0$ and 0.5) measured at room temperature. The inset graph denotes the enlarged part of *M–H* loops under the low field.

the combination of mixed-valent magnetic cations in equal ratio enable the double-exchange interaction to take place [6,10]. The possibility of Mn ions to form the multiple valence states of Mn^{3+}/Mn^{4+} further allows the existence of this interaction. As the molten-salt method was used, the formation of Mn^{4+} ions might be due to the oxide ion donor mechanism involving oxobasic SO_4^{2-} anions from sulfate salts, as explained by Lux-Flood acid-base theory [16,28]. The oxidation of Mn^{3+} is further promoted by the oxygen-rich environment during the high-temperature calcination. The formation of mixed-valent Mn^{3+}/Mn^{4+} in equal proportions was previously reported in Aurivillius compounds synthesized using the molten salt method [9,27]. Thus, the $x = 0.5$ might also contain that Mn^{3+} and Mn^{4+} since it was synthesized using the same molar ratio [16]. The existence of Mn^{4+} ions was in good agreement with the decreased *c* parameter in the refinement result. For the following reasons, we speculate that the possible double-exchange interactions occurring within Mn-rich clusters in the inner $B(1)O_6$ octahedra via Mn(1)-O(1)-Mn(1) bonds, gave rise to the ferromagnetic behavior.

These phenomena were also observed in the four-layer Aurivillius $Pb_{0.4}Bi_{4.6}Ti_{3.4}Mn_{0.6}O_{15}$ resulting in the presence of ferromagnetic interactions with the ferromagnetic-paramagnetic transition temperature (T_c) at 21.49 K [9]. Interestingly, in this sample $Pb_{0.5}Bi_4Nd_{0.5}Ti_{3.5}Mn_{0.5}O_{15}$, the ferromagnetic behavior is still observed at room temperature (300 K), which indicates the improved magnetic properties with the substitution of Nd^{3+} cations for 0.5 mol. It is reported that the ferromagnetic interaction is also correlated with the spin canting of the magnetic ions via the antisymmetric Dzyaloshinskii-Moriya (DM) interaction [29]. According to the recent studies, this spin canting effects can be achieved by substitution of Ln^{3+} cation with a smaller ionic radius on the *A*-site, leading to the smaller bond angles and shorter bond length and hence the enhanced magnetic properties [30,31]. Compared with the $Pb_{0.4}Bi_{4.6}Ti_{3.4}Mn_{0.6}O_{15}$ compound, the substitution of smaller Nd^{3+} (1.27 Å) for Bi^{3+} (1.31 Å) in our current sample induce a higher distortion and a shorter bond length of $Mn(1)O_6$ octahedra, which likely favor enhanced magnetic properties. This result confirms that the combination of *A*- and *B*-site cation substitution is a feasible way to enhance the dielectric as well as the magnetic properties in the Aurivillius phase. We noted that the above discussion is preliminary and requires further study to reveal the magnetic mechanism.

4. Conclusions

The single-phase of the four-layer Aurvillius $Pb_{1-x}Bi_{3.5+x}Nd_{0.5}Ti_{4-x}Mn_xO_{15}$ ($x = 0$, 0.1, 0.3 and 0.5) was successfully obtained by the molten salt method using K_2SO_4/Na_2SO_4 fluxes. The structural analysis confirmed that all the samples adopted the non-centrosymmetric orthorhombic symmetry with the $A2_1am$ space group and the cell volume decreased as the *x* composition increased. The FTIR spectra indicated that the Mn^{3+} ions occupied the *B*-site of perovskite layers. The anisotropic plate-like grain morphology was observed for all samples. The dielectric constant increased with increasing *x* composition, which indicated the increase in ferroelectricity. The ferroelectric polarization arises mainly from the displacement of the *A*- and *B*-site cation along the *a*-direction, according to the orthorhombic $A2_1am$ symmetry. The magnetic investigation for the highest Mn-composition sample ($x = 0.5$) indicated a ferromagnetic behavior, which is assumed to arise from the double-exchange involving the short-range Mn^{3+}-*O*-Mn^{4+} bonds in the inner *B* $(1)O_6$ octahedra structure. The best dielectric properties were obtained for $x = 0.5$ sample, which was at 1 MHz and RT provided a maximum dielectric constant of 245.1 and a dielectric loss (tan δ) of 0.291. This sample also exhibited the ferromagnetic behavior with the remnant magnetization (M_r) of 0.005 emu/g at RT. The coexistence of ferroelectricity and ferromagnetism with the simultaneous substitution of Nd^{3+} and Mn^{3+} for $PbBi_4Ti_4O_{15}$ was expected to provide a potential multiferroic material for the applications in memory storage devices.

CRediT authorship contribution statement

Zulhadjri: Conceptualization, Methodology, Writing - original draft, Validation. **Tio Putra Wendari:** Investigation, Visualization, Writing - original draft. **Upita Septiani:** Investigation, Formal analysis. **Syukri Arief:** Writing - review & editing.

Declaration of competing interest

The authors declare that they have no known competing financial interests or personal relationships that could have appeared to influence the work reported in this paper.

Acknowledgments

This work was supported by the Ministry of Research, Technology and Higher Education (RISTEKDIKTI) of the Republic of Indonesia through the Fundamental Grant with contract number 051/SP2H/LT/DRPM/2019.

References

[1] J.F.Scott, Ferroelectric Memories, first ed., Springer-Verlag Berlin Heidelberg, New York, n.d. doi:10.1007/978-3-662-04307-3.

[2] W. Eerenstein, N.D. Mathur, J.F. Scott, Multiferroic and magnetoelectric materials, Nature 442 (2006) 759–765, https://doi.org/10.1038/nature05023.

[3] A.J.C. Buurma, G.R. Blake, T.T.M. Palstra, Multiferroic Materials : Physics and Properties, Elsevier Ltd., 2016, https://doi.org/10.1016/B978-0-12-803581-8.09245-6.

[4] B. Aurivillius, Mixed bismuth oxides with layer lattices 1. The structure type of $CaNb_2Bi_2O_9$, Ark. För Kemi. 1 (1949) 463–480.

[5] Y. Shu, Q. Ma, Z. Ding, L. Cao, X. Chen, F. Yang, X. Zeng, Multiferroic behaviors of Co-doped $Bi_4NdTi_3FeO_{15}$ ceramics, Phys. Lett. 383 (2019) 911–914, https://doi.org/10.1016/j.physleta.2018.12.031.

[6] R. Ti, C. Wang, H. Wu, Y. Xu, C. Zhang, Study on the structural and magnetic properties of Fe/Co co-doped $Bi_4Ti_3O_{12}$ ceramics, Ceram. Int. 45 (2019) 7480–7487, https://doi.org/10.1016/j.ceramint.2019.01.040.

[7] Z. Yin, Y. Sheng, G. Ma, Dielectric, multiferroic and magnetodielectric properties of Co/Fe co-doped – $Bi_4Ti_3O_{12}$ ceramics, J. Mater. Sci. Mater. Electron. 30 (2019) 10483–10490, https://doi.org/10.1007/s10854-019-01391-0.

[8] C.C. Chou, C.L. Huang, S. Mukherjee, Q.Y. Chen, H. Sakurai, A.A. Belik, H.D. Yang, Multiple magnetic transitions in multiferroic $BiMnO_3$, Phys. Rev. B 80 (2009) 184426, https://doi.org/10.1103/PhysRevB.80.184426.

[9] Zulhadjri, B. Prijamboedi, A.A. Nugroho, N. Mufti, A. Fajar, T.T.M. Palstra, Ismunandar, Aurivillius phases of $PbBi_4Ti_4O_{15}$ doped with Mn^{3+} synthesized by molten salt technique: structure , dielectric , and magnetic properties, J. Solid State Chem. 184 (2011) 1318–1323, https://doi.org/10.1016/j.jssc.2011.03.044.

[10] Y. Shi, Y. Pu, J. Li, W. Wang, R. Shi, M. Yang, X. Guo, X. Wang, J. Ji, X. Peng, Q. Zhang, L. Guo, Dielectric, optical, and multiferroic properties of Co-doped $SrBi_2Nb_{1.8}Fe_{0.2}O_9$ ceramics, J. Mater. Sci. Mater. Electron. 31 (2020) 4719–4731, https://doi.org/10.1007/s10854-020-03028-z.

[11] A. Khokhar, P.K. Goyal, O.P. Thakur, A.K. Shukla, K. Sreenivas, Influence of lanthanum distribution on dielectric and ferroelectric properties of $BaBi_{4-x}La_xTi_4O_{15}$ ceramics, Mater. Chem. Phys. 152 (2015) 13–25, https://doi.org/10.1016/j.matchemphys.2014.11.074.

[12] L. Sheng, X. Du, Q. Chao, P. Zheng, W. Bai, L. Li, F. Wen, W. Wu, L. Zheng, Enhanced electrical properties in Nd and Ce co-doped $CaBi_4Ti_4O_{15}$ high temperature piezoceramics, Ceram. Int. 44 (2018) 18316–18321, https://doi.org/10.1016/j.ceramint.2018.07.044.

[13] Zulhadjri, J.I. Bilian Sahiga, W.T. Putra, Emriadi, Synthesis and structural analysis of aurivillius phase, $Ca_{1-x}Bi_{3+x}NdTi_{4-x}Mn_xO_{15}$, Res. J. Chem. Environ. 22 (2018).

[14] Zulhadjri, A.A. Billah, T.P. Wendari, Emriadi, U. Septiani, S. Arief, Synthesis of aurivillius phase $CaBi_4Ti_4O_{15}$ doped with both La^{3+} and Mn^{3+} cations: crystal structure and dielectric properties, Mater. Res. 23 (2020), e20190521, https://doi.org/10.1590/1980-5373-MR-2019-0521.

[15] H. Chen, B. Shen, J. Xu, L. Kong, J. Zhai, Correlation between grain sizes and electrical properties of $CaBi_2Nb_2O_9$ piezoelectric ceramics, J. Am. Ceram. Soc. 95 (2012) 3514–3518, https://doi.org/10.1111/j.1551-2916.2012.05327.x.

[16] T.P. Wendari, S. Arief, N. Mufti, J. Baas, G.R. Blake, Zulhadjri, Ratio effect of salt fluxes on structure, dielectric and magnetic properties of La,Mn-doped $PbBi_2Nb_2O_9$ Aurivillius phase, Ceram. Int. 46 (2020) 14822–14827, https://doi.org/10.1016/j.ceramint.2020.03.007.

[17] S. Chandel, P. Thakur, M. Tomar, V. Gupta, A. Thakur, Investigation of structural, optical, dielectric and magnetic studies of Mn substituted $BiFeO_3$ multiferroics, Ceram. Int. 43 (2017) 13750–13758, https://doi.org/10.1016/j.ceramint.2017.07.088.

[18] R.D. Shannon, Revised effective ionic radii and systematic studies of interatomie distances in halides and chaleogenides, Acta Crystallogr. 32 (1976) 751–767.

[19] J. Tellier, P. Boullay, M. Manier, D. Mercurio, A comparative study of the Aurivillius phase ferroelectrics $CaBi_4Ti_4O_{15}$ and $BaBi_4Ti_4O_{15}$, J. Solid State Chem. 177 (2004) 1829–1837, https://doi.org/10.1016/j.jssc.2004.01.008.

[20] T.P. Wendari, S. Arief, N. Mufti, V. Suendo, A. Prasetyo, J. Baas, G.R. Blake, Zulhadjri, Synthesis, structural analysis and dielectric properties of the double-layer Aurivillius compound $Pb_{1-2x}Bi_{1.5+2x}La_{0.5}Nb_{2-x}Mn_xO_9$, Ceram. Int. 45 (2019) 17276–17282, https://doi.org/10.1016/j.ceramint.2019.05.285.

[21] J. Yuan, R. Nie, Q. Chen, D. Xiao, J. Zhu, Structural distortion, piezoelectric properties, and electric resistivity of A-site substituted Bi_3TiNbO_9-based high-temperature piezoceramics, Mater. Res. Bull. 115 (2019) 70–79, https://doi.org/10.1016/j.materresbull.2019.03.019.

[22] A.B. Missyul, I.A. Zvereva, T.T.M. Palstra, A.I. Kurbakov, Double-layered Aurivillius-type ferroelectrics with magnetic moments, Mater. Res. Bull. 45 (2010) 546–550, https://doi.org/10.1016/j.materresbull.2010.02.002.

[23] D.Y. Suárez, I.M. Reaney, W.E. Lee, Relation between tolerance factor and Tc in Aurivillius compounds, J. Mater. Res. 16 (2001) 3139–3149, https://doi.org/10.1557/JMR.2001.0433.

[24] Ismunandar, B.A. Hunter, B.J. Kennedy, Cation disorder in the ferroelectric Aurivillius phase $PbBi_2Nb_2O_9$: an anamolous dispersion X-ray diffraction study, Solid State Ionics 112 (1998) 281–289, https://doi.org/10.1016/S0167-2738(98)00222-7.

[25] S.M. Blake, M.J. Falconer, M. Mccreedy, P. Lightfoot, Cation disorder in ferroelectric Aurivillius phases of the type $Bi_2ANb_2O_9$ (A=Ba, Sr, Ca), J. Mater. Chem. 7 (1997) 1609–1613.

[26] Y. Luo, Comprehensive Handbook of Chemical Bond Energies, first ed., CRC Press, Boca Raton, 2007 https://doi.org/10.1201/9781420007282.

[27] T.P. Wendari, S. Arief, N. Mufti, A. Insani, J. Baas, G.R. Blake, Zulhadjri, Structural and multiferroic properties in double-layer Aurivillius phase $Pb_{0.4}Bi_{2.1}La_{0.5}Nb_{1.7}Mn_{0.3}O_9$ prepared by molten salt method, J. Alloys Compd. 820 (2020) 153145, https://doi.org/10.1016/j.jallcom.2019.153145.

[28] J. Boltersdorf, N. King, P.A. Maggard, Flux-mediated crystal growth of metal oxides: synthetic tunability of particle morphologies, sizes, and surface features for photocatalysis research, CrystEngComm 17 (2015) 2225–2241, https://doi.org/10.1039/c4ce01587h.

[29] S. Liu, S. Yan, H. Luo, L. Yao, Z. Hu, S. Huang, L. Deng, Enhanced magnetoelectric coupling in La-modified $Bi_5Co_{0.5}Fe_{0.5}Ti_3O_{15}$ multiferroic ceramics, J. Mater. Sci. 53 (2018) 1014–1023, https://doi.org/10.1007/s10853-017-1604-6.

[30] Z. Yu, X. Meng, Z. Zheng, Y. Lu, H. Chen, C. Huang, H. Sun, K. Liang, Z. Ma, Y. Qi, T. Zhang, Room temperature multiferroic properties of rare-earth-substituted Aurivillius phase $Bi_5Ti_3Fe_{0.7}Co_{0.3}O_{15}$ ceramics, Mater. Res. Bull. 115 (2019) 235–241, https://doi.org/10.1016/j.materresbull.2019.04.002.

[31] J. Li, Y. Pu, X. Wang, Y. Shi, R. Shi, M. Yang, W. Wang, X. Guo, X. Peng, Effect of yttrium doping on the structure, dielectric multiferroic and magnetodielectric properties of $Bi_5Ti_3FeO_{15}$ ceramics, J. Mater. Sci. Mater. Electron. 31 (2020) 4345–4353, https://doi.org/10.1007/s10854-020-02992-w.